IOSR Journal of VLSI and Signal Processing (IOSR-JVSP)
Volume 7, Issue 4, Ver. II (Jul. - Aug. 2017), PP 19-30
e-ISSN: 2319 – 4200, p-ISSN No. : 2319 – 4197
www.iosrjournals.org

Technologies beyond Moore's Law: Simulation results of Heuristic Model

R C Saarvani[1], K Suresh Kumar[2], Rudra Mukesh Reddy[3]
[1]*ECE, SSJ Engineering College, India*
[2] *Assoc Prof, ECE, SSJ Engineering College, India*
[3]*University of Texas at Tyler, Texas*
Corresponding Author: R C Saarvani

Abstract : *Moore's law will eventually reach its limits as complementary metal-oxide semiconductors (CMOS) are reaching their maturity around the year 2020.There is a need for new chip manufacturing techniques to enable the continuation of law The electronics design needs to shift towards devices that are not only minutely small but increasingly capable and scalable. Memristor devices are an important component in fulfilling these needs. In order to be used effectively in the analysis, design and simulation of memristor based circuits it is important that it should be modeled properly. Previous memristor models incorporated a tunnel barrier model but they employed a time rate change in tunnel width which was strictly based on empirical fitting with memristor data. This paper covers our work in developing heuristic model and discussing its performance.*
Keywords: *memristor, heuristic model.*

Date of Submission: 31-07-2017 Date of acceptance: 25-08-2017

I. Introduction

For three decades the semiconductor industry has been able to follow the performance curve known as Moore's law [1]. This law proposed by Gordon Moore of Intel Corporation predicts the maximum number of components, that is, transistors, on a chip will roughly double every 18 months [2]. There is a need for new techniques to enable continuation of the law [5]. Memristor nano-devices are an important component in fulfilling these needs [6, 7].They can be scaled down to less than 10nm and offer fast, nonvolatile, low energy electrical switching [8]. "Memristor", is a two-terminal passive element in which flux is related to the amount of charge that has passed through the device [9]. The existence of memristor is predicted in a paper written by Leon O. Chua in 1971 [10]. The memristor is the fourth basic circuit element because it cannot be built using standard linear circuit elements [11].Leon O. Chua recognized that from the set of four basic electrical variables voltage (v), current (i), charge (q) and magnetic flux ( ),the link between flux and charge is missing he termed it as fourth basic circuit element. This element has become known as a memristor and its symbol is shown in Fig.2. In practice this leads to the property that the device's resistance should vary according to the amount of charge that passed through it and it would remember the final value of resistance even after the current is turned off [11]. Leon O. Chua not only predicted the existence of the memristor but also provided a guide for its electrical characterization. One of its fundamental identifiers is the "pinched hysteresis loop" seen when memristor current is plotted versus an applied sinusoidal voltage (Fig.3)[12]. There is a generalization leading to a complexity metric of circuit elements which not only incorporates the four basic circuit elements but also other memory devices such as memcapacitors [13] and meminductors [13].

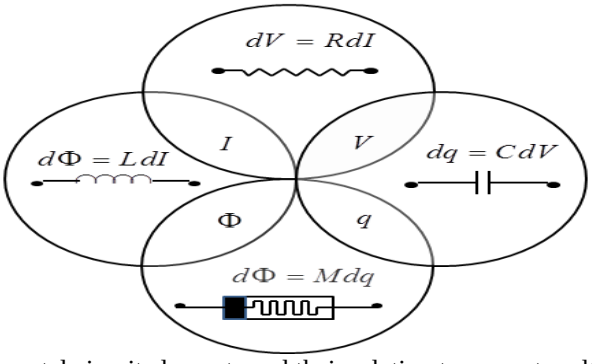

Fig.1 The four fundamental circuit elements and their relation to current, voltage, charge and flux

Fig.2. Memristor symbol [11]

Interest among scientists and engineers worldwide was ignited when it was announced in 2008 by Hewlett Packard (HP) Corporation that they fabricated a physical device with memristor properties [11]. Memristors are expected to have variety of integrated circuit applications such as high speed switches [11], neural hardware [14], high density random access memory (RAM) based on a cross-bar design [12] and digital logic operation [15]. The research is in progress to include memristor crossbar arrays for hardware security [16].

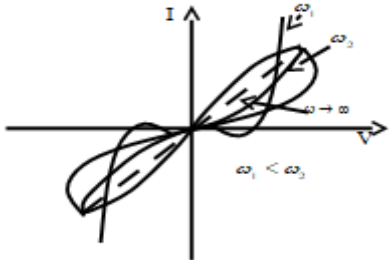

Fig.3. High and low frequency response on memristor *I-V* curve [12].

II. Background

The physical memristor construction, proposed by HP consists of a metal insulator metal structure [12, 11]. HP's memristor design employed a thin film of rutile titanium dioxide (TiO_2) sandwiched between platinum (Pt) contacts (Fig.4). To convert this structure to a working memristor a onetime process is needed, known as electroforming. The unit cell of pure titanium dioxide is developed in SPARTAN (Fig.5).

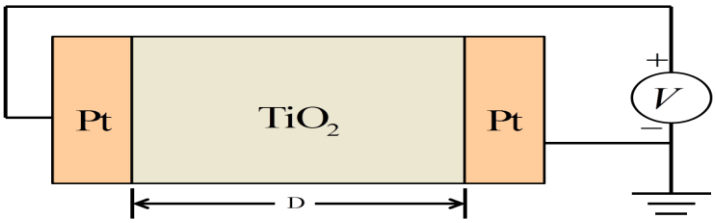

Fig.4 Device before electroforming

SPARTAN is a molecular modeling and computational chemistry application. The unit cell of titanium dioxide consists of two atoms of titanium and four oxygen atoms. There is one body-centered titanium atom and eight shared titanium atoms at the corners of the unit cell. There are two oxygen atoms inside the unit cell and four oxygen atoms on the cell faces. The calculations for titanium are,

#Ti/unit cell= $1+(8/8)=2$ atoms per cell (1)

and for oxygen are,

#O/unit cell= $2+(4/2)=4$ atoms per cell (2)

Electroforming occurs as a onetime application of high-voltage or current that produces a significant increase in the electronic conductivity [11]. The electroforming of the titanium dioxide based memristor is done by varied processes. The electroforming reported in [17] used an external voltage sweep from 0 up to -20V (negative forming) or +10V (positive forming). Also voltage sweep from 0 to +6V over 5ns has been reported [18]. Electrostatic forces generated during electroforming pull the oxygen ions (O^{-2}) away from the neutral cells creating vacancies.

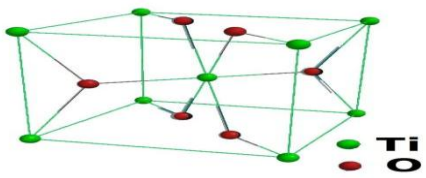

Fig.5 Unit cell of rutile titanium dioxide

The reaction which removes the oxygen vacancy is a redox reaction. The redox reaction near cathode is given below in Kroger-Vink notation [8].

$$Ti^{4+} + ne^{-} \leftrightarrow Ti^{(4-n)+} \tag{3}$$

The oxygen ions (O^{-2}) which are negatively charged will move to the anode and leave Ti^{4+} in the cathode region reduced. Oxidized oxygen ions are released out as oxygen gas near anode. The Kroger-Vink notation for this process is given below [8].

$$O_O \leftrightarrow V_{\ddot{O}} + 2e^{-} + \frac{1}{2}O_2 \tag{4}$$

O_O is the oxygen in a regular cell site and $V_{\ddot{O}}$ is positively charged oxygen vacancy. The doped and undoped regions in titanium dioxide are created by electroforming the device in its rutile TiO_2 state. This destructive process creates a switching center by creating a junction between doped and undoped regions. At the vacancy level, during electroforming oxygen vacancies are created and begin to drift towards the cathode. These form conducting channels in oxide often referred to as magneli phases Ti_4O_7. As described earlier, O^{-2} ions move towards the anode where they evolve as oxygen gas. This causes physical deformation of the junction. After electroforming, the device resistance decreases by several orders of magnitude. The magneli phases are identified to be conducting filaments. Kope et al. identified that after electroforming vacancies can be in multiple arrangements as shown in Fig.6. The vacancy arrangements are labeled R1, R2, R3 and F in Figure 6. In full chain of ordered vacancies the electron localization on the vacancy sites become negligible, thus most electrons localize on the Ti ions between the two cell vacancies, and form a Ti chain of metallic bond.

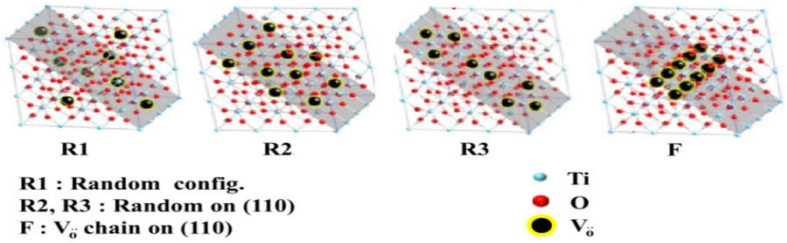

Fig.6 Vacancies in multiple arrangements after electroforming

The switching center is formed at the interface between the two region's location at w_0 identified in Figure 7. The stoichiometric TiO_2 region has exactly 2:1 oxygen to titanium atoms ratio. The TiO_{2-x} region consists of fixed oxygen vacancies which is 2 to 3% [11]. At the completion of electroforming the x is approximately 0.05 [12]. The TiO_{2-x} exhibits higher conductivity. Jameson et al. and Dong et al. identified the field-driven drift of oxygen vacancies is responsible for modulating the Schottky barrier at electrodes. Kope et al. concluded the oxygen vacancies act as mediators of the electron conduction, while the actual electron conduction is through the successive Ti ions in the channel. Only a small percentage (<5%) of the cells within the doped region are affected by electroforming leaving high percentage (95%) in a neutral state [11]. This observation supports the existence of a relatively high, approximately constant, background resistivity in both doped and undoped sections of the device. Including the background resistivity is one added feature specific to conservation of mobile vacancies model (i.e., LNLDM). The oxygen deficient region is termed doped region because its effect is the same as that of added impurities that lower the resistance.

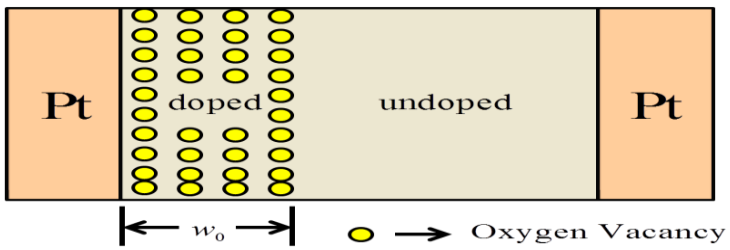

Fig.7 Device immediately after electroforming

The electrical bias convention for analysis of the memristor in the operation mode is shown in Fig.8 [12]. Under memristor operating mode conditions (Fig.8) in which the bias voltage is made positive the electrostatic forces will cause the positively charged vacancies to drift towards the cathode. Upon positive bias it is expected that the drift process will expand the doped region width while the negative bias will lead to a subsequent contraction in the doped region width. This is qualitatively represented with three memristor bias

conditions in Fig.8 [12]. As a consequence of vacancy drift under positive bias the doping section width *w* will expand. In terms of atoms, this drift process is equivalent to a transfer of a negative oxygen ion from a neutral cell into a vacancy of an adjacent cell located on the anode side. The vacancies are marked as (+) in the Fig.8

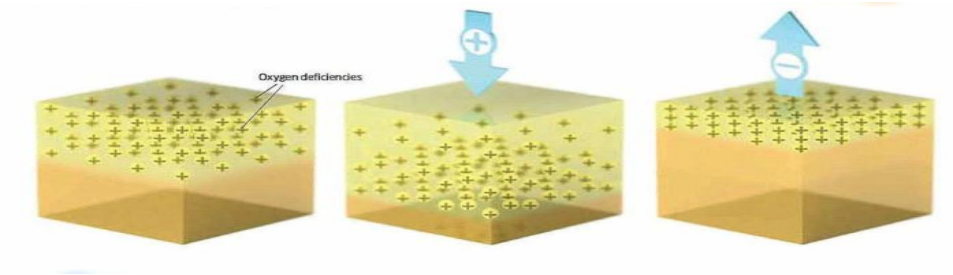

Fig.8 Mechanism of memristor operation [12]

In nano-scale devices, small voltages can yield enormous electric fields, which in turn can produce significant nonlinearities in ionic transport and results in complexity of conduction process of titanium oxide memristors. Research with a focus on the mechanism for electrical conduction has been central to memristor modeling challenges since the advent of the first memristor. There are two distinct mechanisms to characterize the conductive propositions of memristor operation in the literature; they are DDM [11] and TBM .

2.1 Dopant Drift Model

DDM is proposed based on the formation and drift of oxygen vacancies in memristor. As described earlier when an electric field is applied, the oxygen vacancies drift depending on bias polarity, changing the boundary between the high resistance and low resistance layers.

2.1.1 General rules

The general rules used in memristor modeling are presented in this section. According to Faraday's law, the voltage-current relation is,

$$v(t)=M(w)\times i(t)=\frac{d\phi}{dt} \tag{5}$$

where *v(t)* is voltage, $i(t)$ is current and ϕ is the magnetic flux. The memristor quantity known as memristance, $M(w)$ is the effective resistance and is a function of width of the doped region, w, and is,

$$M(w)=R_d(w)+R_{ud}(w) \tag{6}$$

where $R_d(w)$ and $R_{ud}(w)$ are the resistances of the doped and undoped regions of the memristor respectively. Equation (6) is consistent with a series interpretation for the doped and undoped memristor domains. In terms of limits on memristance, the following conditions are applicable,

$$R_{off}=R_{ud}(w=0)=M(w=0) \tag{7a}$$

and ,

$$R_{on}=R_d(w=D)=M(w=D) \tag{7b}$$

and the memristance at the start, i.e., $t=0$ of operating mode satisfies,

$$R_o\equiv M(w=w_o) \tag{8}$$

An application of ohm's law can be used to predict the uniform electric field E_{doped} in the doped region,

$$E_{doped}=\frac{R_d(w)\times i(t)}{w(t)} \tag{9}$$

Assuming a constant mobility, μ_{vac}, the boundary separating doped and undoped regions is dictated by the speed of vacancies [11],

$$\frac{dw}{dt}=\mu_{vac}\times E_{doped}=\mu_{vac}\times\frac{R_d(w)i(t)}{w(t)} \tag{10}$$

The measure for the maximum field strength assuming 100% doped conditions, $w=D$, is

$$E_{\max}=\frac{v_o}{D} \tag{11}$$

where V_o is the peak amplitude for an applied voltage (12) and ω is source frequency.

$$v(t) = v_0 \sin(\omega t) \tag{12}$$

A measure of minimum time it takes boundary to move through distance D is,

$$t_o = \frac{D}{\mu_{vac} E_{\max}} = \frac{D^2}{\mu_{vac} \times V_o} \tag{13}$$

The measure for the amount of charge required to pass through the memristor in the time it takes the dopant boundary w to move through distance *D* is,

$$Q_o = t_o \times i_{\max} = t_o \times \frac{V}{R_{on}} = \frac{D^2}{\mu_{vac} \times R_{on}} \tag{14}$$

A notation simplification used in previous memristor analysis is to express results in terms of normalized doped width [11],

$$x(t) = w(t) / D \tag{15}$$

where $x(t)$ is normalized width for the doped region.

2.1.2 Linear Drift Model (LDM)

The LDM considers linear drift of the oxygen vacancies. According to the LDM [11] the memristance is given by [11],

$$M(w) = R_{on} \frac{w(t)}{D} + R_{off} \left(1 - \frac{w(t)}{D}\right) \tag{16}$$

Comparing (16) with first and second terms (6) identifies $R_d(w)$ and $R_{ud}(w)$ respectively. The resistance of the doped region R_d for the LDM is,

$$R_d = \rho_d \frac{w(t)}{A} = R_{on} \frac{w(t)}{D} \tag{17}$$

where,

$$R_{on} = \frac{\rho_d D}{A} \tag{18}$$

Equations (17-18) are consistent with a constant resistivity (ρ_d) in the doped region. Another form (16) for the LDM often used is,

$$M(w,t) = R_{on} x(t) + R_{off} \left(1 - x(t)\right) \tag{19}$$

To extract the dependence for the location of the interface between doping and non-doping regions w in $q(t)$ substitute (17) back into (10) and integrate with respect to time. After integration the boundary location between doped and undoped regions is,

$$w(t) = w_o + \frac{\mu_{vac}}{D} R_{on} q(t) \tag{20a}$$

where ,

$$q(t) = \int_0^t i(t)dt + q(0) \tag{20b}$$

Equation (20a) shows explicit dependence of width on the time dependent charge. A solution has been developed for the LDM. An analysis based on previously reported relates the differential of flux $\phi(t)$ with the differential of charge $q(t)$,

$$d\phi = d\left[R_o q(t) + \frac{q(t)^2 \Delta R}{Q_o} \right] \tag{21}$$

and with initial conditions $q(t=0) = 0$, and $\phi(t=0) = 0$. The solution to LDM is ,

$$q(t) = \frac{Q_o R_o}{\Delta R} \left[1 - \sqrt{1 - \frac{2\Delta R}{Q_o R_o^2} \phi(t)} \right] \tag{22}$$

where $\Delta R = \left(R_{off} - R_{on}\right)$ and R_o is effective memristance at time t=0. The memristor current can then obtained using (20a) (5). The magnetic flux associated with time rate change of the voltage applied is $\phi(t) = v_0\left(1-\cos(\omega t)\right)/\omega$ using (5) (12). The simulations for LDM.

2.2 TBM

The TBM modeling for memristor is an accurate treatment for conduction phenomenon. The previous sections discussed about tunneling with a static width of insulator, but to model a memristor a dynamic thickness of insulator is required. Pickett et al. [43] gave details of the electroforming process and proposed equations to describe the vacancy dynamics in titanium oxide memristors. Abdalla et al. [45] integrated the time rate change of tunnel gap width given by Pickett with Simmons tunneling equations and created a SPICE model. The device is a thin film of stoichiometric titanium oxide that is sandwiched between two platinum electrodes as shown in Figure 1. It is then electroformed by applying a voltage sweep from 0 to 6 V over 5ms. At the same time, oxygen vacancies are formed, which result in a highly conductive channel called magneli phases (Ti_4O_7) and shunt most of the oxide film except for a narrow tunnel gap as shown in Figure 9. The gap is modeled by an electron tunnel barrier. The tunnel barrier width $\delta(t)$ can be modulated by applying a voltage across the memristor, and the highly conductive channel can be regarded as a resistor $R_s = 215\Omega$. The reported value for R_s is for specific fabricated device with dimensions Pt(15)/TiO_2(50)/Pt(30). The numbers in parentheses are the layers thickness in nanometers. Therefore, after the process of electroforming, the device is equivalent to an Ohmic resistor and a tunnel barrier connected in series as shown in Fig.10.

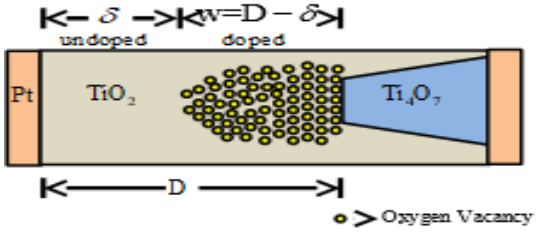

Fig.9 Schematic diagram of a memristor after electroforming

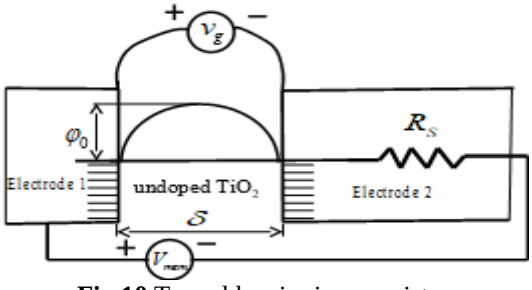

Fig.10 Tunnel barrier in memristor

The current through the device is modeled by using Simmons tunneling junction equation, and its function form is given by (23) [44]. Simmons set of equations are from (25) to (31) and (23).

$$i_{mem} = \frac{j_0 A}{\Delta\delta^2}\left(\bar{\varphi}_{\mathrm{Imem}}\exp\left(-B\bar{\varphi}_{\mathrm{Imem}}^{\frac{1}{2}}\right) - \left(\bar{\varphi}_{\mathrm{Imem}} + qv_g\right)\times\exp\left[-B\left(\bar{\varphi}_{\mathrm{Imem}} + qv_g\right)^{\frac{1}{2}}\right]\right) \tag{23}$$

where the voltage across the tunnel gap is calculated using,

$$v_g = V_{mem} - i_{mem}R_s \tag{24}$$

The Simmons equations used in this memristor model are,

$$j_0 = \frac{q}{2\pi h} \tag{25}$$

$$\delta_1 = 1.2\lambda\delta/\varphi_0 \tag{26}$$

$$\delta_2 = \delta\left[1 - 9.2\lambda / \left(3\varphi_0 + 4\lambda - 2qv_g\right)\right] + \delta_1 \tag{27}$$

$$\Delta\delta = \delta_2 - \delta_1 \tag{28}$$

$$\bar{\varphi}_{Imem} = \varphi_0 - \left(q\mathrm{v}_\mathrm{g} / 2\delta\right)(\delta_1 + \delta_2) - \left[1.15\lambda\delta / \left(\delta_2 - \delta_1\right)\right] \times \ln\left[\frac{\delta_2(\delta - \delta_1)}{\delta_1(\delta - \delta_2)}\right] \tag{29}$$

$$B = 4\pi\Delta\delta\sqrt{2m}/h \tag{30}$$

$$\lambda = q^2 \ln 2 / 8\pi\varepsilon_o K\delta \tag{31}$$

where K is the dielectric constant, h is Planck's constant, m the mass of the electron, A is the channel area of the memristor, q the electron charge, V_{mem} the voltage applied to the tunnel barrier and highly conductive channel, v_g the voltage across the tunnel barrier, φ_0 the barrier height in electron volts and is obtained using numerically fitting techniques by Pickett et al. [43], and ε_0 is the vacuum permittivity. In Figure 10 the series resistor R_s is the result of highly conducting channel formed during electroforming. The tunnel barrier width $\delta(t)$ is time-varying and could be modeled according to the exponential dependence of the switching time on the device current, for off switching $\left(i_{mem} > 0\right)$:

$$\dot{\delta} = f_{off} \sinh\left(\frac{i_{mem}}{i_{off}}\right) \exp\left(-\exp\left(\frac{\delta - a_{off}}{w_c} - \frac{|i_{mem}|}{b}\right) - \frac{\delta}{w_c}\right) \tag{32a}$$

for on switching $\left(i_{mem} < 0\right)$ [43]:

$$\dot{\delta} = f_{on} \sinh\left(\frac{i_{mem}}{i_{on}}\right) \exp\left(-\exp\left(-\frac{\delta - a_{on}}{w_c} - \frac{|i_{mem}|}{b}\right) - \frac{\delta}{w_c}\right) \tag{32b}$$

where f_{off}, i_{off}, a_{off}, b, w_c, f_{on}, i_{on} and a_{on} are all constants. The input parameters are consistent with. The values for these parameters are obtained by numerical fitting procedures.

III. models

3.1 HYBRID MODEL (Background Model)

The DDM and TBM have been introduced in the previous sections. This section examines a unique hybrid combination of best of both the models[13]. The driving force for this model is the existence of numerically fitted, non physical parameters in $d\delta/dt$ equation (32a)(32b) used to model memristor using TBM. The Simmons equations used in the TBM are close to the physical mechanism, but $d\delta/dt$ has its limits with physical background of device. The DDM strength is at vacancy level and can model the dw/dt without the need of having nonphysical, curve fitted parameters. Hence this work examines the hybrid combination of integrating Simmons current equations and dw/dt from DDM. Also the conservation of mobile charge vacancies is applied to the model. The TBM has strict restrictions on the width of the tunnel gap. If input voltages are different from the standard inputs the device could not be modeled. The model proposed in this work solves this issue and forces no limits on the width of the tunnel gap and works well for varied inputs. The model presented in this paper takes the advantages of the Simmons tunneling equations described in TBM (23) for calculating current. The set of equations described by Simmons are for a static thickness of insulator (25-31). The proposed model makes a hybrid set of equations using the Simmons set of equations and calculates $d\delta/dt$ from the laws of DDM. The proposed memristor hybrid model approach is shown in Fig.11.

Memristor with two electrodes (i.e., platinum is one electrode and the other electrode is Ti_4O_7), is a result of electroforming and is shown in Fig.11. The oxygen vacancies are accumulated at the Ti_4O_7 electrode. During operation of memristor these vacancies can drift as explained in DDM. The parameter δ is the thickness of undoped region and is given as input to the Simmons equations for the calculation of memristor current. Let

the device length is $D = (10nm)$ [11], hence length of doped region is given by $w=D-\delta$. According to constant background resistivity proportional to normalized parameter x_{hybrid} is,

$$R_d = \left(R_{on} x_{\text{hybrid}}{}^2\right) || R_{off} x_{\text{hybrid}} \tag{33}$$

where normalized parameter x_{hybrid} is,

$$x_{\text{hybrid}} = w/D = (D-\delta)/D \tag{34}$$

The circuit model is shown in Fig.11 R_s represents series resistor due to magneli phases. The doped and undoped regions shown in Fig.11 indicate the incorporation of the LNLDM. In Fig.11, doped region resistance is a parallel architecture with $R_{on}x^2{}_{hybrid}$ and $R_{off}x_{hybrid}$ resistors. The undoped region resistance is indicated by $\left(1-x_{hybrid}\right)R_{off}$ in Fig.11. R_{on} is the memristor resistance under the conditions the doped region is completely expanded, i.e., $\delta \cong 0 \delta \cong 0$ and the background resistivity is so high it is not impacting the parallel resistance of the doped region. The R_{off} is the memristor resistance under the conditions the undoped region is completely expanded, i.e., $\delta \approx D \delta \approx D$. Neglecting $R_{off}x_{\text{hybrid}}$, equation (33) becomes,

$$R_d \approx R_{on} x^2_{hybrid} R_d \approx R_{on} x^2_{hybrid} \tag{35}$$

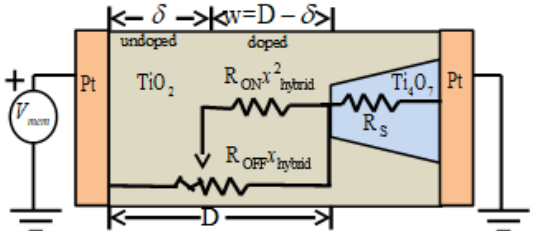

Fig.11 Circuit model for hybrid model

The relation between w, δ, D is,

$$\delta + w = D \tag{36}$$

Differentiating above equation (36) with time,

$$\frac{d\delta}{dt} = -\frac{dw}{dt} \tag{37}$$

The dw/dt for the new model is,

$$\frac{dw}{dt} = -\mu_{vac} \times E_{doped} \tag{38}$$

The negative sign is because, in this model doped region width is measured in reference to the negative electrode. LDM, it is measured from the positive electrode. The electrical field in doped region for the hybrid model is,

$$E_{doped} = \frac{R_d \times i(t)}{D - \delta(t)} \tag{39}$$

Substituting (35) and (38) in (37), we have,

$$\frac{d\delta}{dt} = \mu_{vac} \times \frac{R_{on}\left(D - \delta(t)\right) \times i(t)}{D^2} \tag{40}$$

This $d\delta/dt$ in equation (40) is passed to the Simmons equations for modeling memristor. The total set of equations (23, 2.5-31) from TBM and $d\delta/dt$ in (40) are required to model memristor according to presented hybrid model. An asymmetry in the time rate change dynamics due to coulombic repulsion among positive vacancies as the doped region is compressed is neglected in this model.

3.2 Heuristic Model (Proposed model)

This model uses equations presented in Section 3.1, and achieves maximum correlation between simulations and the experimental values published. The model described in Sections 3.1 are good to operate on symmetrical inputs. Due to the symmetrical inputs for the model described in Sections 3.1 the width of the tunnel gap returns to the initial value after completion of the cycle and therefore device can be modeled successfully for more than one cycle. The dynamics of the width of the tunnel gap varies linearly for on and off switching.. The model proposed in this section is partially based on heuristics to achieve this effect. This method also tries to make the model compatible with asymmetric inputs. The reasoning this model uses is to match the dynamics of width of tunnel gap δ to the dynamics simulated for tunnel barrier width of TBM. The dynamics of the tunnel barrier gap for TBM simulated in LTspice are shown in Fig.12. In off switching the dynamics of tunnel barrier width indicate a smooth increase. A sudden sharp decrease is observed in on switching around 4.5sec. To achieve this effect in HTM an extra term is added to Equation (39),

$$E_{doped} = \frac{R_d \times i(t)}{D - \delta(t)} - \frac{\alpha \times \sqrt{(D - \delta(t))}}{D^2} \tag{41}$$

where $\alpha \simeq 0.01$ was obtained through trial and error method to yield reasonable agreement with memristor device data. The E_{doped} term (41) is integrated for the positive half of input waveform. The term is then given as an impulse of equal area after three quarters of the input wave form (i.e., 75% to 80% of the input waveform). The reason for applying the term as an impulse is because the $d\delta/dt$ simulated for TBM indicated smooth increase in off switching and an impulsive response in the on switching. The on and off switching for $d\delta/dt$ are derived from $\delta(t)$ as in Fig.12, are shown in Fig.13.

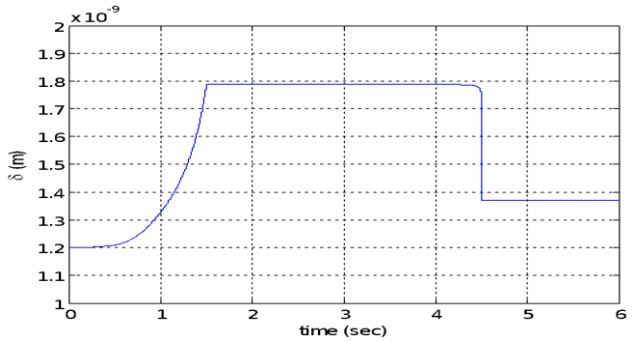

Fig.12 Dynamical behavior of tunnel barrier width TBM

In Fig.12, time interval 0-3 seconds corresponds to on switching and 3-6 sec corresponds to off switching. In on switching the temporal variation in $d\delta/dt$ indicates a smooth increase till 0-1.5 sec and remains constant at zero until 3 sec. In off switching $d\delta/dt$ remains constant at zero except a sudden impulse is observed at time interval close to 4.5 sec. These dynamics indicate that vacancies in off switching move closer to Ti_4O_7 electrode and there is an increase in vacancy concentration. Hence this effect cause vacancies to form more concentrated Ti-Ti bonds. When device enters off switching some energy is required to break this concentrated Ti-Ti and once the long Ti-Ti bonds break, the field causes them to move towards other electrode as discussed earlier. Hence the impulse applied relates to this process.

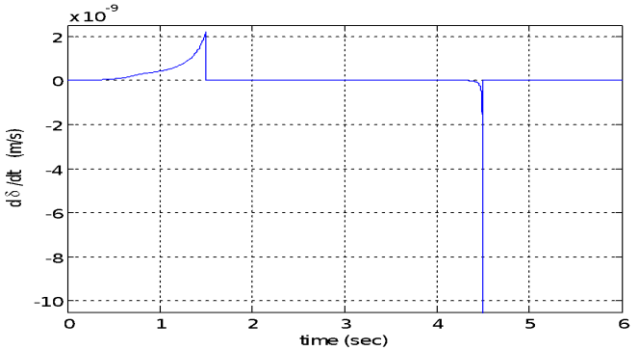

Fig.13 The temporal variation in $d\delta/dt$ for TBM simulated in Matlab

IV. simulation results

4.1 Simulation results for Heuristic model

In this section simulations for HTM are presented. The heuristics model background is described in above section. The HTM has been applied a triangular signal as shown in Fig.14. This peculiar input is applied because the *I-V* characteristics of the model are later compared with the experimental device. This model forces an impulsive response in the $d\delta/dt$.

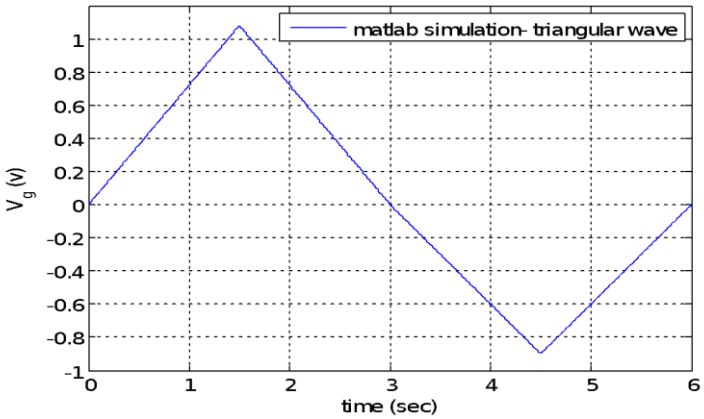

Fig.14 The input triangular wave applied to HTM in Matlab

The *I-V* characteristics obtained for triangular wave are shown in Fig.15. The experimental data points are also plotted to compare the model. The comparison between HP data points and HTM are in accordance as shown in Fig.15. Due to the asymmetric applied signal the hysteresis is also asymmetric. The current i_{mem} reaches 2 mA at 1.5 V of voltage across memristor v_{mem} in off switching. In on switching the current i_{mem} reaches 1 mA at 0.95 V of voltage across memristor v_{mem} . The temporal change in tunnel barrier width is shown in Fig.16. The nonlinear behavior observed is inherently built into equations. In comparison to off switching time the on switching is faster. This is consistent with on and off switching observed in Fig.12. The device returns back to its initial state hence this model can be simulated over more than one input cycle, unlike the nonlinearity observed in the Abdalla model. This model introduces the non-linearity due to changes in field due to contractions and spread of oxygen vacancies. This effect due to oxygen vacancies modulates the electric field in doped region and is shown in Fig.17. In Fig.17 it can be seen the electric field in doped region gradually increases at the start of the cycle. This is when the device is in its off state switching i.e., width of the tunnel barrier starts increasing. As width of the tunnel barrier is increasing the width of the doped region starts decreasing. the oxygen vacancies start to accumulate near the magneli phases (Ti_4O_7) (Fig.11). It is possible that in the compression process the concentrated chains of Ti-Ti metallic bonds are beginning to form. In the on state switching of the memristor, [3 sec- 6 sec] there is an impulse in electric field. The impulse may be because the concentrated Ti-Ti metallic bonds need some energy to break the bond.

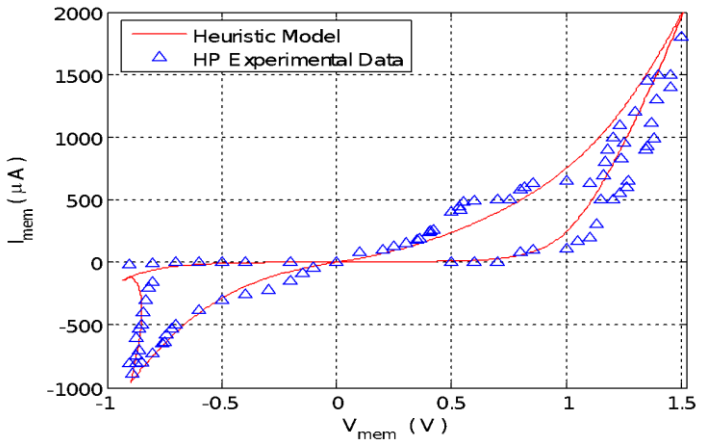

Fig.15 Comparison between HTM and experimental data points

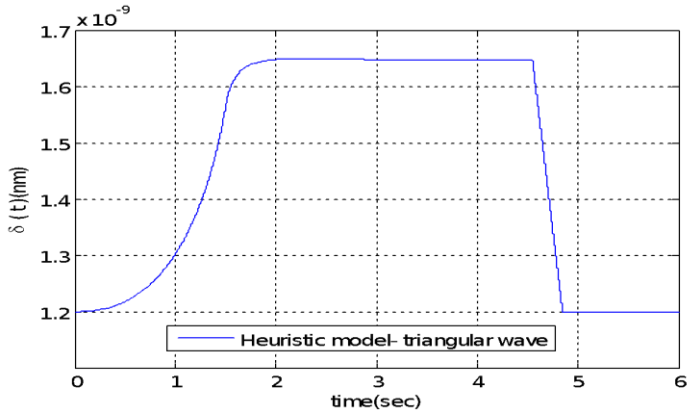

Fig.16 The width of tunnel barrier $\delta(t)$ simulated in Matlab for HTM

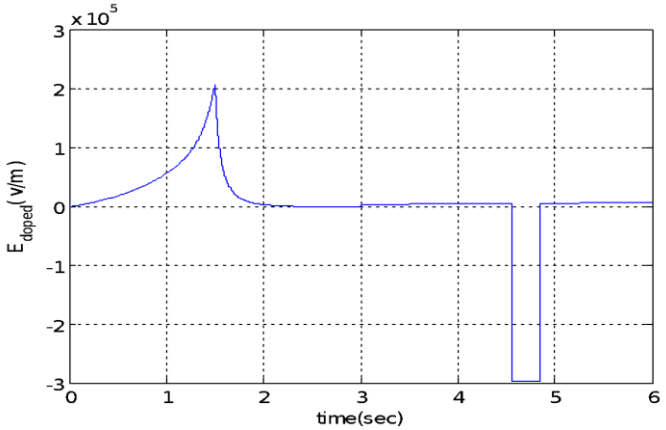

Fig.17 The temporal variations in electric field in doped region for HTM

Once the bonds are broken the vacancies can respond to the electric field, hence, with $d\delta/dt$ negative the width of the tunnel barrier decreases. This phenomenon is observed from the dynamics of the tunnel barrier width shown in Fig.16. The described effect is built into the model by including an additional term in (9) which results in (41). The time rate change of tunnel barrier width is shown in Fig.18. In Fig.18, the $d\delta/dt$ starts increasing from 0 to 1.5 sec and decreases for 1.5 to 3 sec. In the on switching of the device the impulse is applied at 4.4 sec to 4.8 sec. The position and interval of the impulse is a result of iterative approach.

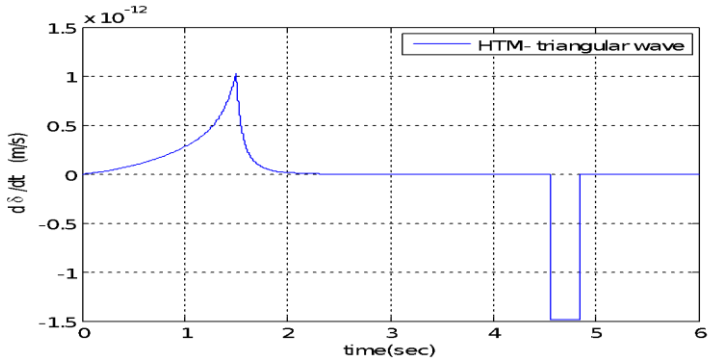

Fig.18 The time rate change for tunnel barrier width in HTM

V. Conclusion

The Hybrid model has the flexibility in amplitude variation. The width of the tunnel gap reaches its initial state after one complete cycle of applied waveform. Hence the model can be operated with multiple cycles of applied waveform. The Hybrid model widths demonstrated symmetric switching dynamics, heuristic model solves this issue, heuristic model results are in perfect agreement with the experimental data points provided by HP. The heuristic model recreated the lip phenomenon observed in the HP experimental data for *I-V* characteristics.

References

[1] P. K. Bondyapadhyay, "Moore's Law Governs the Silicon Revolution," Proceedings of the IEEE, vol.86, no.1, pp.78-81, January 1998.
[2] G. E. Moore, "Cramming more Components onto Integrated Circuits," Electronics, vol.38, no.8, April 1965.
[3] B. G. Streetman and S. K. Banerjee, "Integrated Circuits," Solid State Electronic Devices, 6th ed. New Jersey, USA: Princeton Hall, 2006, ch.9, sec.2, pp.441.
[4] http://www.extremetech.com/computing165331-intels-former-chief-architect-moores-law-will-be-dead-within-a-decade, accessed on March 28, 2014.
[5] R. K. Cavin, P. Lugli and V. V. Zhirnov, "Science and Engineering Beyond Moore's Law," Proceedings of IEEE, vol.100, pp.1720-1749, May 2012.
[6] S. Tyagi, "Moore's Law: A CMOS Scaling Perspective," 14th International Symposium on the Physical and Failure Analysis of Integrated Circuits (IPFA), Bangalore, India, pp.10-15, 2007.
[7] Z. Jing and H. Da, "The Influences of Model Parameters on the Characteristics of Memristors," Chinese Phys. B, vol.21, no.4, pp.1-10, April 2012.
[8] J. J. Yang, D. B. Strukov and D. R. Stewart, "Memristive Devices for Computing," Nature Nanotechnology, vol.8, no.1, pp.13-22, January 2013.
[9] L. O. Chua, "Introduction to Nonlinear Network Theory," New York: McGraw-Hill, 1969.
[10] L. O. Chua, "Memristor-The Missing Circuit Element," IEEE Transactions on Circuit Theory, vol.18, no.5, pp.507–519, Sep 1971.
[11] D. B. Strukov, G. S. Snider, D. R. Stewart and R. S. Williams, "The Missing Memristor Found," Nature, vol.453, no.7191, pp.80-83, May 2008.
[12] R. S. Williams, "How we Found the Missing Memristor," IEEE Spectrum, vol.45, no.12, pp.1-6, 2008.
[13] L. O. Chua, "The Fourth Element," IEEE proceedings, vol.100, no.6, pp.1920-1927, June
[14] M. R. Rudra, & R. J. Pieper, "Memristor characteristics via an integration of drift and tunnel barrier models,"IETE Journal of Research, vol.61, no.4, pp.440-443, April 2015.

IOSR Journal of VLSI and Signal Processing (IOSR-JVSP) is UGC approved Journal with Sl. No. 5081, Journal no. 49363.

R C SaarvaniTechnologies beyond Moore's Law: Simulation results of Heuristic Model." IOSR Journal of VLSI and Signal Processing (IOSR-JVSP) , vol. 7, no. 4, 2017, pp. 19-30.